

# A quantum coprocessor for accelerating simulations of non-equilibrium many body quantum dynamics

J. M. Kreula,<sup>1,\*</sup> S. R. Clark,<sup>2,3</sup> and D. Jaksch<sup>1,4</sup>

<sup>1</sup>Clarendon Laboratory, University of Oxford, Parks Road, Oxford OX1 3PU, United Kingdom

<sup>2</sup>Department of Physics, University of Bath, Claverton Down, Bath BA2 7AY, United Kingdom

<sup>3</sup>Max Planck Institute for the Structure and Dynamics of Matter, Hamburg, Germany

<sup>4</sup>Centre for Quantum Technologies, National University of Singapore, 3 Science Drive 2, Singapore 117543

(Dated: October 20, 2015)

Next generation scalable quantum devices<sup>1</sup> promise a step change in our ability to do computations. Direct quantum simulation<sup>2</sup> using highly controllable quantum systems has already led to numerous insights into many body quantum physics, despite limitations in the size of the simulated system<sup>6</sup>. Here we propose a hybrid simulator for the non-equilibrium dynamics of strongly correlated infinite quantum lattices based on ideas from non-equilibrium dynamical mean field theory (DMFT)<sup>2,3</sup>. Our scheme uses a quantum coprocessor to efficiently solve a linear impurity problem with parameters iterated to self-consistency via a feedback loop evaluated on a classical computer. The required quantum resources scale linearly with the simulated time while known classical algorithms scale exponentially. Quantum gate errors can partly be accounted for in the classical feedback loop improving the simulation results. We thus conclude that current efforts to develop scalable quantum technologies<sup>1,6,7</sup> have the potential to outperform classical non-equilibrium DMFT simulations in the near future.

Strongly correlated quantum systems driven out of thermal equilibrium exhibit some of the most intriguing physical phenomena like light-induced superconductivity<sup>8</sup>. The underlying physical mechanisms are, however, still poorly understood. Even conceptually simple and commonly used quantum lattice models are often not fully grasped. They are extremely challenging to study numerically due to the exponential growth in Hilbert space with system size. One thus often resorts to mean field approximations which typically consider only a single lattice site and replace interactions with its neighbourhood by a mean field  $\Lambda_\sigma$ , with spin  $\sigma = \uparrow, \downarrow$ , as schematically shown in Figs. 1a,b. This mean field approximation becomes increasingly accurate with the number of nearest neighbours  $z$ , i.e. the coordination number of the lattice. A classic example of this approach is the Weiss mean-field theory for explaining ferromagnetism<sup>9</sup>. For mean field theory to be applicable to strongly correlated Fermi systems in thermal equilibrium,  $\Lambda_\sigma(t)$  has to be dynamical in order to account for correlations between interactions with the environment that are separated by  $t$  in time. This highly successful approach is called DMFT<sup>2</sup>. DMFT can be extended to

non-equilibrium systems<sup>3</sup> by letting  $\Lambda_\sigma(t, t')$  depend on two interaction times  $t$  and  $t'$  explicitly.

Determining  $\Lambda_\sigma(t, t')$  and the related local single-particle Green's function  $G_\sigma(t, t')$ , which describes the response of the many-body system after a localized removal and addition of a particle at times  $t'$  and  $t$ , is a complex task. Commonly used numerical methods for solving the non-equilibrium DMFT problem include continuous-time quantum Monte Carlo, which suffers from a severe dynamical sign problem, and perturbation theory which can only address the weak and strong coupling regimes<sup>3</sup>. Here we follow a different approach<sup>4</sup> and map the system onto a single impurity Anderson model (SIAM) where the selected lattice site is represented by an impurity whose interaction with the field  $\Lambda_\sigma(t, t')$  is mimicked by a collection of  $N$  non-interacting baths with energies  $\epsilon_{p\sigma}(t)$  as shown in Fig. 1c. Dynamical hybridization energies  $V_{1p}^\sigma(t)$  describe the exchange of fermions between the impurity site and the bath sites. These must be determined self-consistently: for given  $V_{1p}^\sigma(t)$  the quantum dynamics of the SIAM is solved and its mean field  $\Lambda_\sigma(t, t')$  and corresponding Green's function are determined; from these a new set of  $V_{1p}^\sigma(t)$  can be worked out which is then fed back into the SIAM. These steps are repeated until convergence is achieved<sup>4</sup>. The dynamics of the SIAM is usually worked out by exact diagonalization (ED)<sup>4</sup> for small systems or tensor network theory (TNT) methods<sup>5</sup>. However, the dynamical generation of entanglement in these problems has severely hampered the efficiency TNT methods<sup>5,12</sup>. Furthermore, the required number of bath sites  $N$  usually increases linearly with the maximum simulation time  $t_{\max}$ , which makes solving this problem exponentially difficult<sup>4,5,13</sup> in  $t_{\max}$  using classical methods.

In this Letter, we analyze a hybrid quantum-classical computing scheme to efficiently solve strongly correlated quantum lattice models based on the idea of DMFT. A small digital quantum coprocessor solves the linear dynamical SIAM with the resulting  $\Lambda_\sigma(t, t')$  being processed by a classical computer to complete the non-linear feedback loop as shown in Fig. 1d. We show that already a coprocessor of approximately 50 qubits can outperform current classical computations. Moreover, even for imperfectly implemented quantum gates with realistic errors of 1% we find accurate solutions to a simple model problem in small systems. In addition, our numerical evidence suggests that gate errors mainly lead to a smearing of the bath energies, which can be incorporated into the

feedback loop to improve the solution further.

Figure 2 shows the quantum network computed by the coprocessor. The impurity state  $\hat{\rho}_{\text{imp}}$  is stored by two qubits whose computational basis states represent the four possible local states  $\{|\text{vac}\rangle, |\uparrow\rangle, |\downarrow\rangle, |\uparrow\downarrow\rangle\}$  of a spin- $\frac{1}{2}$  fermionic site. The real and imaginary parts of the impurity Green's function are encoded as  $\langle\sigma^z\rangle$  and  $\langle\sigma^y\rangle$  of an ancilla qubit by interacting it with the impurity state at times  $t'$  and  $t$  via controlled quantum gates<sup>9</sup> (see Methods for details). The unitary dynamics of the SIAM can be decomposed into a network of quantum gates<sup>7,8</sup>. We first decompose the evolution by discretising time as  $t_n = n\Delta t$ , where  $\Delta t$  is a small time-step, and breakup evolution e.g. from  $t = 0$  to  $t = t_n$  as product of Trotter steps  $\hat{U}(t_n, 0) = \prod_n \hat{U}(n \rightarrow n+1)$ , with a Trotter error  $\propto \Delta t^2$  compared to the exact SIAM evolution. For concreteness we here consider a coprocessor realized by an ion trap<sup>6,7</sup>. The Trotter steps can readily be implemented by single qubit rotations  $\hat{U}_{\text{rot}}(\varphi)$  where  $\varphi$  is the angle of rotation, and multi-qubit entangling Mølmer-Sørensen (MS) gates<sup>8,17</sup> which have been recently realized in ion traps with high fidelity<sup>6</sup>. The total number of MS gates per Trotter step scales linearly with the number of bath sites  $N$ .

We analyze the performance of the coprocessor by considering the infinite-dimensional time-dependent Hubbard model in a Bethe lattice with constant onsite interaction  $U$  and tunneling matrix element  $v(t)$ . The simulation starts in the half-filled paramagnetic atomic limit with tunneling  $v(t=0) = 0$  which is then dynamically ramped up to its final value  $v_0$  after quench time  $1/4v_0$  and is kept at  $v_0$  until the final simulation time  $t_{\text{max}}^4$  (setting  $\hbar = 1$ ). Such a sudden quench is representative of experimental ultracold atom dynamics<sup>18</sup> and also ultrafast dynamics probed in condensed matter systems<sup>1</sup>. We emulate the operation of the quantum coprocessor by classically evaluating the quantum network. The self-consistency condition for the Bethe lattice calculated in the classical feedback loop is  $\Lambda_\sigma(t, t') = v(t)G_\sigma(t, t')v(t')$  from which we obtain the SIAM couplings via a Cholesky decomposition  $\Lambda_\sigma(t, t') = \sum_p V_{1p}^\sigma(t)V_{1p}^\sigma(t')$  (see Supplementary Material for details). The impurity site double occupancy  $\langle\hat{d}\rangle(t) = \langle\hat{n}_\downarrow\hat{n}_\uparrow\rangle(t)$  obtained from the self-consistent hybrid simulation is compared to the exact result in Fig. 3a and shows that the Trotter error does not noticeably affect our results.

Next we assume imperfect gates with phase errors of the form  $\hat{U}_{\text{rot}}(\varphi + \epsilon)$  and  $\hat{U}_{\text{MS}}^{l,m}(\theta + \epsilon_{\text{MS1}}, \phi + \epsilon_{\text{MS2}})$ , where  $\epsilon$ ,  $\epsilon_{\text{MS1}}$ , and  $\epsilon_{\text{MS2}}$  are normally distributed random variables with zero mean. We choose their standard deviations consistent with current experimental capabilities<sup>1,6,20</sup>  $\sigma = 10^{-6}$  and allow  $\sigma_{\text{MS1}} = \sigma_{\text{MS2}} \equiv \sigma_{\text{MS}}$  to vary between 0.1% and 10%.

We obtain accurate results for the dynamics of the double occupancy even in the presence of gate errors. As shown in Fig. 3a the double occupation differs from the exact result by only  $\approx 3\%$  for  $\sigma_{\text{MS}} = 1\%$ . For a smaller gate error of  $\sigma_{\text{MS}} = 0.1\%$  the difference is insignificant up

to  $t = 1.5/v_0$ . In Fig. 3b we plot the error in the imaginary part of the lesser Green's function  $G_\sigma^<(t, t')$  induced by imperfect gates. The diagonal values  $G_\sigma^<(t, t)$ , which determine time-local single-particle observables, are almost unaffected even for large MS gate errors. Gate errors in general make the Green's function decay faster with  $t - t'$  than in the ideal case and will thus affect two-time correlation functions.

We investigate the effect of imperfect gates further by considering the impurity site coupled to two bath sites via constant  $V_{1p}^\sigma$ . We find that the imaginary part of the mean field differs from the exact solution by a factor of approximately  $\approx \exp(-\eta|t' - t|)$  as shown in Fig. 4a. The decay rate  $\eta$  increases with  $\sigma_{\text{MS}}$  as displayed in the inset of Fig. 4a. This numerical evidence suggests that gate errors have the same effect as smearing out the bath energies  $\epsilon_{p\sigma}(t)$  to a width  $\eta$ . The impurity model including errors would then be equivalent to the bath sites possessing a finite coherence time  $1/\eta$ . Since the number of gates is  $\propto N$  we expect  $\eta$  to only depend weakly on  $N$ .

A bath site  $p$  with coherence time  $1/\eta$  can be modelled by allowing an ideal bath to incoherently exchange particles with a reservoir at an 'error' rate  $\Gamma = \eta/2$ . This exchange of particles modifies the bath's Green's function from its ideal value of  $g_{p\sigma}(t, t') = 1$  and correspondingly modifies the relation between impurity bath couplings and mean field from a Cholesky decomposition to<sup>4</sup>  $\Lambda_\sigma(t, t') = \sum_p V_{1p}^\sigma(t)g_{p\sigma}(t, t')V_{1p}^\sigma(t')$  which does not necessarily have an exact solution for  $V_{1p}^\sigma(t)$ . The effect of noise therefore limits the mean fields  $\Lambda_\sigma(t, t')$  that the bath sites can model.

We investigate if the noise induced by gate errors can partly be compensated by instead implementing self-consistency via this modified decomposition. For the non-interacting impurity with bath sites coupled to a particle reservoir we solve numerically for the bath Green's functions  $g_{p\sigma}(t, t')$  exploiting the super-fermion formalism<sup>10</sup> (see Supplementary Material). We implement a noise-reduction scheme by replacing the Cholesky decomposition with the minimization of  $\left\| \sum_p V_{1p}^\sigma(t)g_{p\sigma}(t, t')V_{1p}^\sigma(t') - \Lambda_\sigma(t, t') \right\|$  using the Frobenius norm over the  $V_{1p}^\sigma(t)$  to obtain the hybridizations in the noisy system. This way we can significantly reduce the average absolute error in the mean field  $\Lambda_\sigma(t, t')$  using only *classical* numerical techniques, as demonstrated in Fig. 4b. A slight modification of the coprocessor network in Fig. 2 allows the probe qubit to measure the bath Green's functions providing input information for this noise-reduction scheme in the hybrid simulation scheme.

In summary, we have proposed a hybrid quantum-classical simulation algorithm to study non-equilibrium many-body quantum dynamics crucial to current experiments. Being based on a DMFT impurity problem allows the scheme to work directly in the thermodynamic limit where the number of qubits available limits the maximum time  $t_{\text{max}}$  accessible. In contrast, trying to directly quantum simulate a lattice system with the same number of

qubits will suffer from strong finite-size boundary effects. Moreover the scheme has the potential to outperform current classical simulation with near future quantum technology. Purely classical simulations are currently limited to  $\approx 25$  bath sites<sup>5</sup> and still scale exponentially with  $t_{\max}$  because of fast growing entanglement<sup>4,5</sup>. As such a quantum computing device with only 50 qubits<sup>1</sup> coupled to a classical feedback loop would be able to outperform current classical algorithms. The DMFT self-consistency approach also provides some robustness to errors. The effect of errors is to limit the form of mean fields that can be modelled by the quantum coprocessor. Our numerical evidence suggests this can be partly alleviated by modifying the standard classical feedback loop to improve the accuracy of calculations.

The authors would like to thank Simon Benjamin as well as Ian Walmsley and his group members for useful discussions. The research leading to these results has received funding from the European Research Council under the European Union's Seventh Framework Programme (FP7/2007-2013)/ERC Grant Agreement no. 319286 Q-MAC and from the EPSRC National Quantum Technology Hub in Networked Quantum Information Processing. J. M. K. acknowledges financial support from Christ Church, Oxford and the Osk. Huttunen Foundation.

While preparing this manuscript, we became aware of related work by B. Bauer et al<sup>22</sup>.

## Methods

### Implementing the single-impurity Anderson model with the quantum coprocessor

To implement the SIAM with the quantum coprocessor, we first map the fermionic creation and annihilation operators in the SIAM Hamiltonian  $\hat{H}_{\text{SIAM}}$  (see Supplementary Material) onto spin operators that act on the qubits in the coprocessor. This is achieved via the Jordan–Wigner transformation  $\hat{c}_{p\downarrow}^\dagger = \bigotimes_{j=1}^{2p-2} \hat{\sigma}_j^z \otimes \hat{\sigma}_{2p-1}^-$ ,  $\hat{c}_{p\uparrow}^\dagger = \bigotimes_{j=1}^{2p-1} \hat{\sigma}_j^z \otimes \hat{\sigma}_{2p}^-$ , and  $\hat{c}_{p\sigma} = (\hat{c}_{p\sigma}^\dagger)^\dagger$ . Here,  $\hat{\sigma}^\pm = \frac{1}{2}(\hat{\sigma}^x \pm i\hat{\sigma}^y)$ , and  $\hat{\sigma}^x$ ,  $\hat{\sigma}^y$ , and  $\hat{\sigma}^z$  are the Pauli spin operators. The transformation maps  $N$  fermionic sites onto a string of  $2N$  qubits such that two adjacent qubits represent one lattice site. The correspondences between the qubit states and fermionic states are  $|0, 0\rangle = |\text{vac}\rangle$ ,  $|1, 0\rangle = |\downarrow\rangle$ ,  $|0, 1\rangle = |\uparrow\rangle$ , and  $|1, 1\rangle = |\downarrow\uparrow\rangle$ .

To obtain the necessary quantum gates to approximate the unitary evolution operator we use a Trotter decomposition on the propagator  $\hat{U}(n \rightarrow n+1)$  between each time  $t_n$  and  $t_{n+1}$  as  $\hat{U}(n \rightarrow n+1) = e^{-i\Delta t \hat{H}_{\text{SIAM}}(t_n)} \approx \prod_j e^{-i\Delta t \hat{H}_j(t_n)}$ , where  $\hat{H}_{\text{SIAM}}(t_n) = \sum_j \hat{H}_j(t_n)$ . Each term  $e^{-i\Delta t \hat{H}_j(t_n)}$  can be readily implemented using spin rotations  $\hat{U}_{\text{rot}}(\varphi)$  where  $\varphi$  is the angle of rotation, and multi-qubit Mølmer–Sørensen (MS) gates<sup>8,17</sup>, characterized by two phases  $\theta$  and  $\phi$

as  $\hat{U}_{\text{MS}}^{l,m}(\theta, \phi) = \exp\left[-i\frac{\theta}{4}\left(\cos\phi\hat{S}_x + \sin\phi\hat{S}_y\right)^2\right]$ , with  $\hat{S}_{x,y} = \sum_{j=l}^m \hat{\sigma}_j^{x,y}$  (see Supplementary Material). Here, the MS gate acts on qubits  $l, l+1, \dots, m$ , and the phase  $\theta$  controls the amount of entanglement, while varying  $\phi$  allows a shift between a  $\hat{\sigma}^x$  or a  $\hat{\sigma}^y$  type gate.

### Measuring the impurity Green's function with single-qubit interferometry

Using the Jordan–Wigner transformation, the impurity Green's function  $G_\sigma(t, t')$  can be written as a sum of expectation values of products of Pauli operators and the evolution operators (see Supplementary Material). We propose to use a simple single-qubit interferometry scheme<sup>9</sup> to measure each of the expectation values  $L(t, t')$  that constitute the Green's function. We introduce a probe qubit which is coupled to the string of  $2N$  system qubits. We assume that the probe qubit is prepared in the pure state  $|0\rangle$ , yielding the total system-probe density operator  $\hat{\rho}_{\text{tot}} = \hat{\rho}_{\text{sys}} \otimes |0\rangle\langle 0|$ . The combined system is then run through a Ramsey interferometer sequence, in which first a  $\pi/2$  pulse (or Hadamard gate  $\hat{\sigma}_H$ ) is applied to the probe qubit, the state of which will transform into the superposition  $(|0\rangle + |1\rangle)/\sqrt{2}$ . The two states in the superposition provide the necessary interference paths. Following the  $\pi/2$  pulse, we apply the unitary evolution on the system of interest up to a certain time  $t'$ . The Pauli operators are then applied on the system as controlled quantum gates with either  $|0\rangle$  or  $|1\rangle$  as the control state. This is followed by evolution up to the final time  $t'$ , another controlled application of Pauli gates, and finally another  $\pi/2$  pulse is applied on the probe qubit, bringing the interference paths together. The output state of the probe qubit at the end of the Ramsey sequence is given by

$$\begin{aligned} \hat{\rho}_{\text{probe}} &= \text{Tr}_{\text{sys}} \left[ \hat{\sigma}_H \hat{T} \hat{\sigma}_H \hat{\rho}_{\text{tot}} \hat{\sigma}_H \hat{T}^\dagger \hat{\sigma}_H \right] \\ &= \frac{1 + \text{Re}[L(t, t')]}{2} |0\rangle\langle 0| - i \frac{\text{Im}[L(t, t')]}{2} |0\rangle\langle 1| \\ &\quad + i \frac{\text{Im}[L(t, t')]}{2} |1\rangle\langle 0| + \frac{1 - \text{Re}[L(t, t')]}{2} |1\rangle\langle 1|, \end{aligned}$$

where  $L(t, t') = \text{Tr}_{\text{sys}} \left[ \hat{T}_1^\dagger(t) \hat{T}_0(t, t') \hat{\rho}_{\text{sys}} \right]$ . Here, the unitary operators  $\hat{T}_0(t, t') = \langle 0 | \hat{T} | 0 \rangle = \hat{U}(t, t') \hat{\sigma} \hat{U}(t', 0)$  and  $\hat{T}_1(t) = \langle 1 | \hat{T} | 1 \rangle = \hat{\sigma}' \hat{U}(t, 0)$ , in which  $\hat{\sigma}$  and  $\hat{\sigma}'$  are Pauli operators or tensor products of Pauli operators (see Supplementary Material), act only on the system and not on the probe qubit. Note that  $\hat{\rho}_{\text{probe}} = \frac{1}{2} \left( \hat{I} + \text{Re}[L(t, t')] \hat{\sigma}_z + \text{Im}[L(t, t')] \hat{\sigma}_y \right)$ , so that we have  $\text{Tr}_{\text{probe}} [\hat{\rho}_{\text{probe}} \hat{\sigma}_z] = \text{Re}[L(t, t')]$ , and  $\text{Tr}_{\text{probe}} [\hat{\rho}_{\text{probe}} \hat{\sigma}_y] = \text{Im}[L(t, t')]$ . Therefore repeated measurements of the  $\hat{\sigma}_z$  and  $\hat{\sigma}_y$  components of the probe qubit for all times  $t'$  and  $t$  yields the impurity Green function  $G_\sigma(t, t')$ .

- 
- \* Electronic address: j.kreula1@physics.ox.ac.uk
- <sup>1</sup> Nature Phys. **11**, 89 (2015).
- <sup>2</sup> R. P. Feynman, International journal of theoretical physics **21**, 467 (1982).
- <sup>6</sup> R. Blatt and C. F. Roos, Nature Physics **8**, 277 (2012).
- <sup>2</sup> A. Georges, G. Kotliar, W. Krauth, and M. J. Rozenberg, Rev. Mod. Phys. **68**, 13 (1996).
- <sup>3</sup> H. Aoki, N. Tsuji, M. Eckstein, M. Kollar, T. Oka, and P. Werner, Rev. Mod. Phys. **86**, 779 (2014).
- <sup>6</sup> J. Benhelm, G. Kirchmair, C. F. Roos, and R. Blatt, Nature Physics **4**, 463 (2008).
- <sup>7</sup> B. P. Lanyon, C. Hempel, D. Nigg, M. Müller, R. Geritsma, F. Zähringer, P. Schindler, J. T. Barreiro, M. Rabach, G. Kirchmair, et al., Science **334**, 57 (2011).
- <sup>8</sup> D. Fausti, R. I. Tobey, N. Dean, S. Kaiser, A. Dienst, M. C. Hoffmann, S. Pyon, T. Takayama, H. Takagi, and A. Cavalleri, Science **331**, 189 (2011).
- <sup>9</sup> J. Cardy, *Scaling and renormalization in statistical physics*, vol. 5 (Cambridge university press, 1996).
- <sup>4</sup> C. Gramsch, K. Balzer, M. Eckstein, and M. Kollar, Phys. Rev. B **88**, 235106 (2013).
- <sup>5</sup> F. A. Wolf, I. P. McCulloch, and U. Schollwöck, Phys. Rev. B **90**, 235131 (2014).
- <sup>12</sup> J. I. Cirac and P. Zoller, Nature Physics **8**, 264 (2012).
- <sup>13</sup> K. Balzer, Z. Li, O. Vendrell, and M. Eckstein, Phys. Rev. B **91**, 045136 (2015).
- <sup>9</sup> R. Dorner, S. R. Clark, L. Heaney, R. Fazio, J. Goold, and V. Vedral, Phys. Rev. Lett. **110**, 230601 (2013).
- <sup>7</sup> J. Casanova, A. Mezzacapo, L. Lamata, and E. Solano, Phys. Rev. Lett. **108**, 190502 (2012).
- <sup>8</sup> M. Müller, K. Hammerer, Y. L. Zhou, C. F. Roos, and P. Zoller, New Journal of Physics **13**, 085007 (2011).
- <sup>17</sup> K. Mølmer and A. Sørensen, Physical Review Letters **82**, 1835 (1999).
- <sup>18</sup> T. Langen, R. Geiger, and J. Schmiedmayer, Annu. Rev. Condens. Matter Phys. **6**, 201 (2015).
- <sup>1</sup> S. Wall et al., Nature Phys. **7**, 114 (2011).
- <sup>20</sup> T. P. Harty, D. T. C. Allcock, C. J. Ballance, L. Guidoni, H. A. Janacek, N. M. Linke, D. N. Stacey, and D. M. Lucas, Phys. Rev. Lett. **113**, 220501 (2014).
- <sup>10</sup> A. A. Dzhioev and D. S. Kosov, J. Chem. Phys. **134**, 044121 (2011).
- <sup>22</sup> B. Bauer, D. Wecker, A. J. Millis, M. B. Hastings, and M. Troyer, arXiv:1510.03859 (2015).

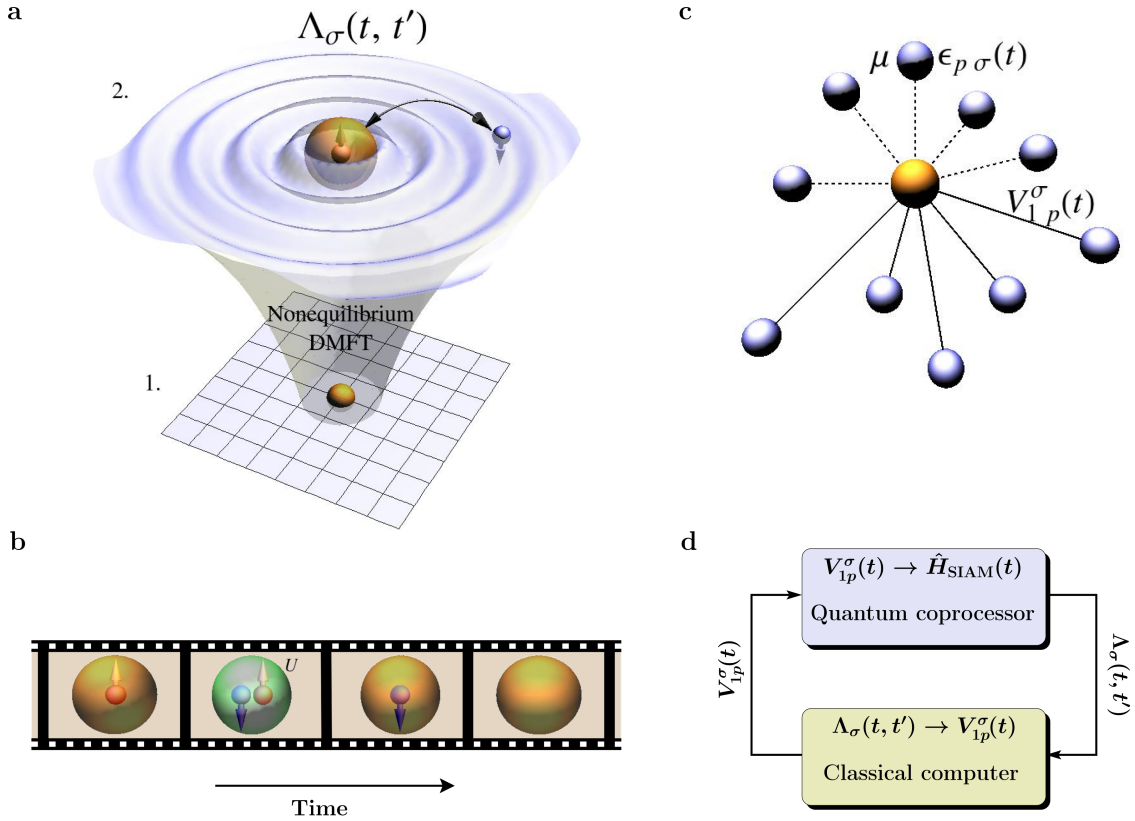


FIG. 1: **a.** In non-equilibrium DMFT a fermionic quantum lattice model is replaced by a single impurity site exchanging particles via a self-consistently determined time and spin dependent mean field  $\Lambda_\sigma(t, t')$ . **b.** This exchange of particles yields dynamical fluctuations of the impurity site occupation as a function of time shown here as  $|\uparrow\rangle \rightarrow |\downarrow\rangle \rightarrow |\downarrow\rangle \rightarrow |\text{vac}\rangle$ . **c.** The impurity - mean field interaction is mapped onto a SIAM with unitary evolution  $U(t, t')$ . The non-interacting bath sites ( $p > 1$ ) energies  $\epsilon_{p\sigma}(t) = 0$  for  $t > 0$  and the chemical potential  $\mu = 0$  in this work<sup>4</sup>. The impurity site exchanges fermions with time-dependent hybridization energies  $V_{1p}^\sigma(t)$ . **d.** Hybrid simulation scheme: the SIAM dynamics for a given set parameters  $V_{1p}^\sigma(t)$  is implemented on a quantum coprocessor and yields the impurity Green's function  $G_\sigma(t, t')$ . The classical non-linear feedback loop takes  $G_\sigma(t, t')$  and calculates the mean field  $\Lambda_\sigma(t, t')$  from which a new set of  $V_{1p}^\sigma(t)$  can be extracted. These parameters are then fed back into the quantum coprocessor and the loop is repeated until self-consistency is achieved.

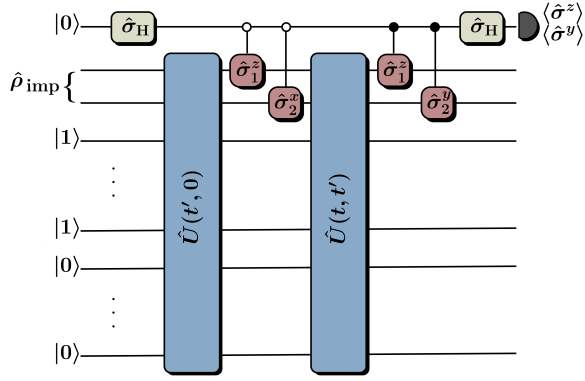


FIG. 2: Coprocessor quantum network for measuring  $G_\sigma(t, t')$  in the SIAM dynamics. A probe qubit (top line) is prepared in  $|0\rangle$  and then put into a symmetric superposition by a Hadamard gate  $\hat{\sigma}_H$ . The lines below the impurity correspond to bath sites whose initial states are chosen to simplify the updates of the  $V_{1p}^\sigma(t)$ <sup>4</sup>. After evolving the impurity to time  $t'$  via the unitary SIAM dynamics  $\hat{U}(t', 0)$  the probe qubit interacts with the impurity site via controlled Pauli gates. A second set of controlled Pauli gates are applied after evolving the impurity further to time  $t$ . The precise choice of Pauli gates selects different contributions to the Green's function. After another Hadamard gate this contribution is encoded in the expectation values  $\hat{\sigma}^z$  and  $\hat{\sigma}^y$  of the probe qubit, as discussed in Methods.

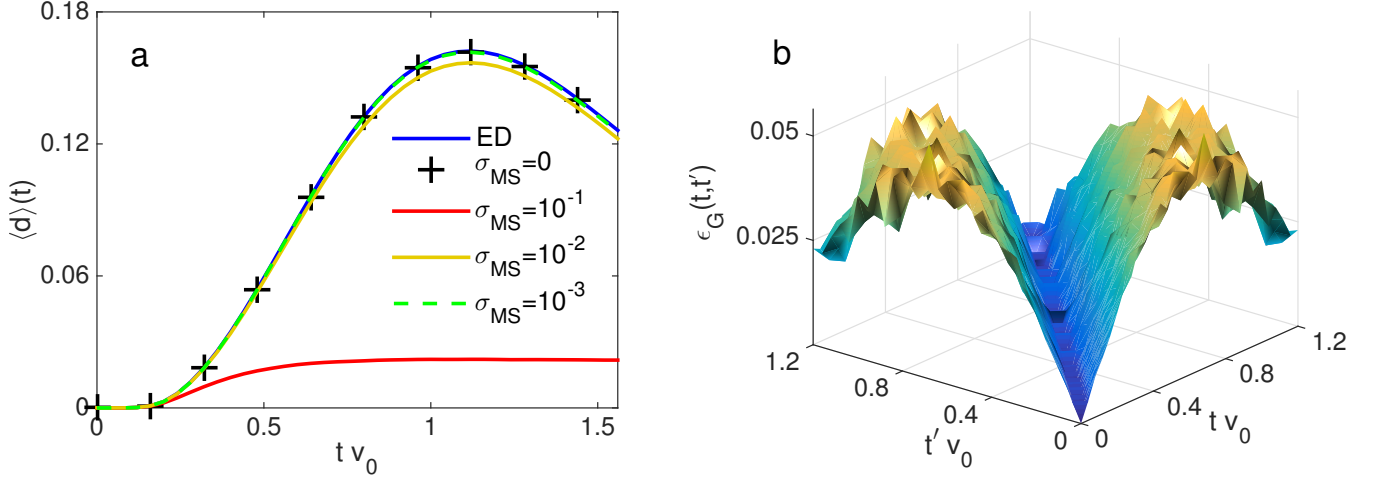


FIG. 3: Hybrid non-equilibrium DMFT simulation results for dynamically increasing the tunneling matrix element  $v(t)$  from 0 to  $v_0$  in the Hubbard model, as described in the main text. We choose  $U = 2v_0$ , Trotter steps  $\Delta t = 0.04/v_0$  and couple the impurity site to  $N = 2$  bath sites. **a.** Impurity double occupation  $\langle \hat{d} \rangle(t)$  as a function of time  $t$ : numerically exact solution (blue solid curve), solution with Trotter errors (black pluses), solutions including gate errors of  $\sigma_{MS} = 10\%$  (red solid curve),  $\sigma_{MS} = 1\%$  (yellow solid curve), and  $\sigma_{MS} = 0.1\%$  (green dashed curve). **b.** Absolute value of the difference  $\epsilon_G(t, t')$  between the imaginary parts of the lesser Green's function without gate errors and with gate errors of  $\sigma_{MS} = 1\%$ . Results of calculations with gate errors are obtained by averaging over 128 realizations.

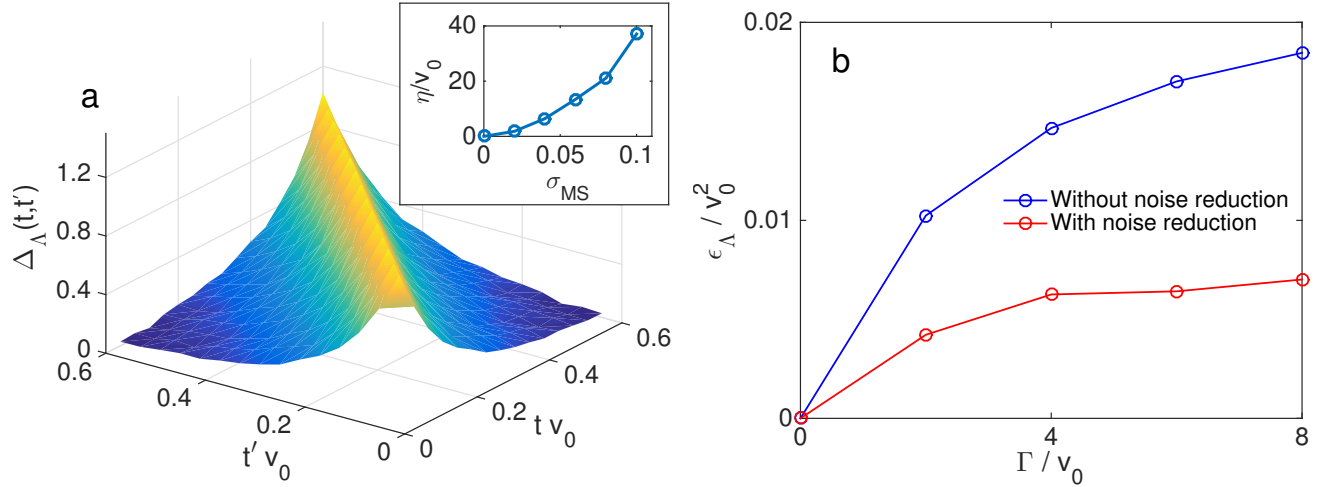


FIG. 4: **a.** Deviation of the mean field  $\Delta_\Lambda(t, t') = \text{Im}\Lambda_{\eta}^<math>\lesssim(t, t') / \text{Im}\Lambda_0^<math>\lesssim(t, t') \approx \exp(-\eta|t - t'|)</math>, where  $\Lambda_{(0, \eta)}^<math>\lesssim(t, t')</math> is the lesser component of the mean field, in the absence (presence) of gate errors (of  $\sigma_{MS} = 6\%$ ) for constant hybridizations and  $U = 2v_0$ ,  $N = 2$  and averaged over 128 realizations. The inset shows the exponential decay rate  $\eta$  against two qubit error  $\sigma_{MS}$ . **b.** Average error in the self-consistent mean field  $\epsilon_\Lambda = |\Lambda_{\text{noisy}}^<math>\lesssim(t, t') - \Lambda_{\text{exact}}^<math>\lesssim(t, t')|</math> for the non-interacting system with  $N = 10$  noisy bath sites. The two curves show a significant reduction in the error when taking the noisy bath Green's functions into account in the classical feedback loop.$$$

## Supplementary material to: “A quantum coprocessor for accelerating simulations of non-equilibrium many body quantum dynamics”

We provide background details on non-equilibrium dynamical mean-field theory and the setup that we study in the main text, and present the formulae needed for implementing the single-impurity Anderson model with qubits and on measuring the single-particle non-equilibrium Green function. We further elucidate the non-interacting system where we studied reducing the effects of a noisy bath.

### Non-equilibrium Dynamical Mean-field Theory

One of the simplest models to capture essential phenomena in strongly-correlated electron materials is the single-band Hubbard Hamiltonian

$$\hat{H}_{\text{Hubbard}} = - \sum_{\langle i,j \rangle \sigma} v_{ij}(t) \left( \hat{c}_{i,\sigma}^\dagger \hat{c}_{j,\sigma} + \text{h.c.} \right) + U(t) \sum_i \left( \hat{n}_{i,\uparrow} - \frac{1}{2} \right) \left( \hat{n}_{i,\downarrow} - \frac{1}{2} \right), \quad (1)$$

where  $v_{ij}(t)$  is the tunnelling (‘hopping’) matrix element between nearest-neighbour sites  $i$  and  $j$ , and  $U(t)$  is the on-site Coulomb repulsion. Here, we have assumed general time-dependent parameters due to the driving of material via, e.g., intense laser pulses<sup>1</sup>. Furthermore,  $\hat{c}_{i,\sigma}^\dagger$  ( $\hat{c}_{i,\sigma}$ ) is the creation (annihilation) operator for an electron with spin projection  $\sigma = \uparrow, \downarrow$  at site  $i$ , while  $\hat{n}_{i,\sigma} = \hat{c}_{i,\sigma}^\dagger \hat{c}_{i,\sigma}$  is the corresponding number operator.

Despite its apparent simplicity, the Hubbard model (1) is notoriously difficult to solve, even numerically, and especially in two dimensions where it may be relevant to high- $T_c$  superconductivity. Fortunately, dynamical mean-field theory (DMFT)<sup>2</sup> and its extension to non-equilibrium problems<sup>3</sup> provide a means to compute local observables by circumventing the necessity of dealing directly with the Hubbard Hamiltonian. This is achieved by mapping it onto an impurity model, the solution of which is usually easier to obtain, albeit still a highly non-trivial computational task. The mapping is justified in the limit of infinite spatial dimensions,  $d \rightarrow \infty$ , (or infinite coordination,  $z \rightarrow \infty$ ) by the collapse of the irreducible self-energy of the Hubbard model to only contributions emerging from strictly local skeleton diagrams which are identical to those of an impurity model. The collapse of the skeleton diagrams follows from the necessity to scale the hopping parameters as  $v_{ij}(t) = v^*/\sqrt{z}$  to avoid a diverging average kinetic energy per lattice site and from simple power counting arguments. While describing the full Hubbard Hamiltonian with a single-impurity model is only an approximation in finite dimensions, it often relatively accurate already in three dimensions for certain lattice types.

The solution of the impurity model means essentially

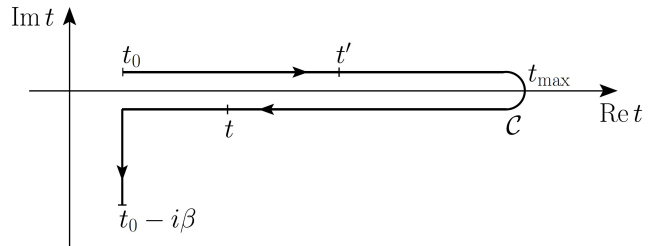


FIG. 5: Keldysh time-contour  $\mathcal{C}$ . It consists of two real-time branches between an initial time  $t_0$  to final time  $t_{\max}$ , and an imaginary-time branch from  $t_0$  to  $t_0 - i\beta$ , where  $\beta$  is the inverse temperature.

computing the local Green function

$$G_\sigma(t, t') = -i \langle \hat{c}_\sigma(t) \hat{c}_\sigma^\dagger(t') \rangle_{\hat{S}_{\text{loc}}} = -i \frac{\text{Tr} \left\{ \mathcal{T}_{\mathcal{C}} \left[ \exp(\hat{S}_{\text{loc}}) \hat{c}_\sigma(t) \hat{c}_\sigma^\dagger(t') \right] \right\}}{\text{Tr} \left\{ \mathcal{T}_{\mathcal{C}} \left[ \exp(\hat{S}_{\text{loc}}) \right] \right\}}, \quad (2)$$

where  $\mathcal{T}_{\mathcal{C}}$  is the contour-ordering operator on an ‘L-shaped’ Keldysh time-contour  $\mathcal{C}$  (see Fig. 5). The local action  $\hat{S}_{\text{loc}}$  is given by<sup>4</sup>

$$\hat{S}_{\text{loc}} = -i \int_{\mathcal{C}} dt \left[ U(t) \left( \hat{n}_\uparrow(t) - \frac{1}{2} \right) \left( \hat{n}_\downarrow(t) - \frac{1}{2} \right) - \mu \sum_\sigma \hat{n}_\sigma(t) \right] - i \int_{\mathcal{C}} dt \int_{\mathcal{C}} dt' \sum_\sigma \Lambda_\sigma(t, t') \hat{c}_\sigma^\dagger(t) \hat{c}_\sigma(t'). \quad (3)$$

Here,  $\mu$  is the chemical potential and  $\Lambda_\sigma$  is the *a priori* unknown hybridization function, or Weiss function, that describes the exchange of electrons between the impurity site with a bath of non-interacting electrons. The essential step in DMFT is the self-consistent determination of  $\Lambda_\sigma$ . For a Bethe lattice, which corresponds to a semi-elliptical density of states  $D(\epsilon) = \sqrt{4v^2 - \epsilon^2}/(2\pi v^2)$ , the DMFT self-consistency condition obtains a simple closed form. For time-dependent hoppings  $v$ , this reads

$$\Lambda_\sigma(t, t') = v(t) G_\sigma(t, t') v(t'). \quad (4)$$

The impurity action (3) can also be represented in a Hamiltonian form which permits the application of Hamiltonian-based numerical methods<sup>4,5</sup> to compute the local Green function. It also makes it possible to use the trapped-ion scheme for quantum simulations<sup>6</sup>. The impurity model that we address here is the single-impurity

Anderson model (SIAM) given by

$$\hat{H}_{\text{SIAM}} = \hat{H}_{\text{loc}} + \hat{H}_{\text{bath}} + \hat{H}_{\text{hyb}}, \quad (5)$$

$$\hat{H}_{\text{loc}} = -\mu \sum_{\sigma} \hat{n}_{1\sigma} + U(t) \left( \hat{n}_{1\uparrow} - \frac{1}{2} \right) \left( \hat{n}_{1\downarrow} - \frac{1}{2} \right), \quad (6)$$

$$\hat{H}_{\text{hyb}} = \sum_{p>1} \left( V_{1p}^{\sigma} \hat{a}_{1\sigma}^{\dagger} \hat{a}_{p\sigma} + \text{H.c.} \right), \quad (7)$$

$$\hat{H}_{\text{bath}} = \sum_{p>1, \sigma} [\epsilon_{p\sigma}(t) - \mu] \hat{a}_{p\sigma}^{\dagger} \hat{a}_{p\sigma}, \quad (8)$$

Here,  $\hat{a}_{p\sigma}^{\dagger}$  ( $\hat{a}_{p\sigma}$ ) is the creation (annihilation) operator for the impurity orbital for  $p = 1$ , and for a bath orbital for  $p > 1$ . Further,  $V_{1p}^{\sigma}$  describes the hopping of electrons between the impurity and the bath, and  $\epsilon_{p\sigma}(t)$  denotes the energy of the bath orbital  $p$ .

The SIAM Hamiltonian (5) corresponds to the correct DMFT action (3) if the parameters  $V_{1p}^{\sigma}$  and  $\epsilon_{p\sigma}(t)$  are chosen such that the relation

$$\Lambda_{\sigma}^{\text{SIAM}}(t, t') = \Lambda_{\sigma}(t, t') \quad (9)$$

is valid on the whole Keldysh contour  $\mathcal{C}$ . Here, the SIAM hybridization function has the expression<sup>4</sup>

$$\Lambda_{\sigma}^{\text{SIAM}}(t, t') = \sum_p V_{1p}^{\sigma}(t) g_{p\sigma}(t, t') V_{p1}^{\sigma}(t'), \quad (10)$$

where

$$g_{p\sigma}(t, t') = i [f(\epsilon_{p\sigma}(0) - \mu) - \Theta_{\mathcal{C}}(t, t')] e^{-i \int_{\mathcal{C}} d\bar{t} (\epsilon_{p\sigma}(\bar{t}) - \mu)} \quad (11)$$

is the non-interacting Green function for an isolated bath site, with  $f(\epsilon) = 1/(\exp(\beta\epsilon) + 1)$  denoting the Fermi distribution function and  $\Theta_{\mathcal{C}}(t, t')$  being the contour Heaviside function defined as

$$\Theta_{\mathcal{C}}(t, t') = \begin{cases} 1 & \text{if } t \geq_{\mathcal{C}} t' \\ 0 & \text{else.} \end{cases} \quad (12)$$

An essential part of the Hamiltonian-based DMFT scheme is the determination of the parameters  $V_{1p}^{\sigma}(t)$  and  $\epsilon_{p\sigma}(t)$  for a given hybridization function  $\Lambda_{\sigma}(t, t')$ . In what follows, we will relax the spin index  $\sigma$  for the hybridization function since below we will be dealing with a spin-symmetric set-up where both contributions are identical.

For non-equilibrium problems, it is useful to introduce two distinct baths, with each having their own corresponding hybridization function<sup>4</sup>. The first bath, with hybridization  $\Lambda_{-}$ , includes those sites that are coupled to the impurity at  $t = 0$ . Often this first bath vanishes as  $t \rightarrow \infty$ . The second bath,  $\Lambda_{+}$ , builds up as time

evolves, i.e., couples additional bath sites to the impurity for times  $t > 0$ . We will consider a system with no initial correlations ( $\Lambda_{-} = 0$ ) in the next section, and focus only on the second bath, with Weiss function

$$\Lambda_{+}(t, t') = \sum_p V_{1p}^{+}(t) g_p(t, t') V_{p1}^{+}(t'). \quad (13)$$

Since all imaginary-time components, which account for initial correlations, vanish for  $\Lambda_{+}$ , we set  $V_{1p}^{+}(t=0) = 0$  for all bath sites that are included in  $\Lambda_{+}$ . The time-dependence of the bath energies  $\epsilon_p(t)$  can be absorbed in the time dependence of the hoppings  $V_{1p}^{+}(t)$ , meaning that we are free to choose the evolution<sup>4</sup>

$$\epsilon_p(t) = \begin{cases} \epsilon_p(0) & \text{for } t = 0 \\ \epsilon(\infty) & \text{for } t > 0 \end{cases}, \quad (14)$$

where  $\epsilon(\infty)$  is a constant. Moreover, since  $\epsilon_p(0)$  is incorporated only in the Fermi functions  $f[\pm(\epsilon_p(0) - \mu)]$  for  $\Lambda_{+}^{</>}$ , we can simply choose  $\epsilon_p(0)$  such that  $f(\epsilon_p(0) - \mu)$  is equal to 0 or 1. This is done in order to find a representation of the Weiss functions as

$$-i\Lambda_{+}^{<}(t, t') = \sum_{p \in B_{\text{occ}}} V_{1p}^{+}(t) V_{p1}^{+}(t')^*, \quad (15)$$

$$i\Lambda_{+}^{>}(t, t') = \sum_{p \in B_{\text{empty}}} V_{1p}^{+}(t) V_{p1}^{+}(t')^*, \quad (16)$$

in which  $B_{\text{occ}}$  and  $B_{\text{empty}}$  denote the sets of initially occupied and empty bath sites, respectively. Note that for a particle-hole symmetric system,  $\Lambda_{+}^{<}(t, t') = \Lambda_{+}^{>}(t, t')^*$ , which is satisfied if the occupied and empty bath sites come in pairs with complex conjugate hybridizations. Moreover, for a discretized time  $t_n = n \times \Delta t \in [0, N \times \Delta t = t_{\text{max}}]$ , we have, e.g.,

$$(-i\Lambda_{+}^{<})_{nn'} = -i\Lambda_{+}^{<}(t_n, t_{n'}) = \sum_{p \in B_{\text{occ}}} V_{1p}^{+}(t_n) V_{p1}^{+}(t_{n'})^*, \quad (17)$$

which has the form of a Cholesky decomposition  $(-i\Lambda_{+}^{<}) = VV^{\dagger}$  where  $V$  is a lower triangular matrix, the  $p$ th column of which gives the time-dependent hybridization to the bath orbital  $p$ . The use of Cholesky decomposition to determine the hybridizations from the Weiss function allows us to adopt a time-propagation scheme in which we do not update the whole Green and Weiss function matrices as time evolves but only the current time slice. In practice, since we only have a limited number of bath sites  $L$ , we employ an approximate representation of the Weiss function in which we obtain the evolution of the first  $L$  time-steps from the Cholesky decomposition, and for time steps greater than  $L$  we update a new column and row in the Weiss function matrix in a manner which minimizes the error in the approximate representation<sup>4</sup>. In the next section we present a test system and use the results of this section to determine the Weiss field self-consistently for the Hubbard model in an infinite-dimensional Bethe lattice.

### The set-up and DMFT steps

We consider the time evolution of the infinite-dimensional Hubbard model with constant on-site interaction  $U$  and time-dependent hopping  $v(t)$ <sup>4</sup>. The hopping is turned on from the initial value  $v = 0$  (i.e., the atomic limit) to the final value  $v = v_0 = 1$ , which we use as the unit of energy, with the profile

$$v(t) = \begin{cases} \frac{1}{2} [1 - \cos(\omega_0 t)] & \text{for } t < t_q \\ 1 & \text{for } t \geq t_q \end{cases}, \quad (18)$$

where  $\omega_0 = \pi/t_q$  and  $t_q > 0$  is a suitable quench time. In our simulations we use  $t_q = 0.25/v_0$ . We assume a zero temperature initial state in the paramagnetic phase in the half-filled Bethe lattice. We then map the Hubbard model onto a SIAM. Since  $v(t=0) = 0$ ,  $\Lambda_-$  vanishes and the hybridization function is given by  $\Lambda = \Lambda_+$ . Since we have a spin- and a particle-hole symmetric system, the bath is represented with pairs of initially occupied and empty sites. We take the total number of bath sites to be  $L_{\text{bath}} = 2L$ , where  $L$  is the rank of the approximate representations of  $-i\Lambda^<$  and  $i\Lambda^>$ . The initial ground state of the SIAM has an equal number of empty and doubly occupied bath sites with energies  $\epsilon_{p\sigma} = 0$ , and singly-occupied impurity which is spin-mixed with density matrix  $\rho_0 = (|\uparrow\rangle\langle\uparrow| + |\downarrow\rangle\langle\downarrow|)/2$ . To account for occupation of the impurity site, we consider two subsystems  $\alpha$  and  $\beta$ , in which the impurity of the system  $\alpha$  ( $\beta$ ) is initially occupied by a single  $\uparrow$ -electron ( $\downarrow$ -electron). We then compute two impurity Green functions  $G_{\text{imp},\sigma}^\alpha$  and  $G_{\text{imp},\sigma}^\beta$  the average of which yields the local lattice Green function

$$G_{\text{loc},\sigma}(t, t') = \frac{1}{2} \left[ G_{\text{imp},\sigma}^\alpha + G_{\text{imp},\sigma}^\beta \right], \quad (19)$$

after self-consistency has been reached. Since we are considering the Hubbard model in the Bethe lattice, the DMFT self-consistency condition is given by Eq. (4).

The non-equilibrium DMFT steps to compute the single-particle lattice Green function for a maximum simulation time  $t_{\text{max}} = N \times \Delta t$  are then the following:

0. Choose an initial Green function  $g_0$ . For iteration  $n = 1$ , initialize the hybridization function as  $\Lambda_1(t, t') = v(t)g_0(t, t')v(t')$ , for  $t, t' \leq t_{\text{max}}$ , where  $v$  is the hopping in the Hubbard Hamiltonian.
1. Use the Cholesky decomposition for  $\Lambda_n$  to obtain the hopping parameters  $V_{1p}(t)$  for the  $n$ th iteration.
2. Use exact diagonalization techniques to compute the impurity Green functions  $G_{\text{imp},\sigma}^{s,\alpha} = \Theta_C(t, t')G_{\text{imp},\sigma}^{s,>}(t, t') + \Theta_C(t', t)G_{\text{imp},\sigma}^{s,<}(t, t')$  for  $s =$

$\alpha$  and  $s = \beta$ , where

$$\begin{aligned} G_{\text{imp},\sigma}^{s,>}(t, t') &= -i\langle\psi_0^s|\hat{U}(0, t)\hat{c}_{1\sigma}\hat{U}(t, t')\hat{c}_{1\sigma}^\dagger\hat{U}(t', 0)|\psi_0^s\rangle, \\ G_{\text{imp},\sigma}^{s,<}(t, t') &= i\langle\psi_0^s|\hat{U}(0, t')\hat{c}_{1\sigma}^\dagger\hat{U}(t', t)\hat{c}_{1\sigma}\hat{U}(t, 0)|\psi_0^s\rangle, \\ \hat{U}(t, t') &= \mathcal{T}e^{-i\int_{t'}^t d\tau \hat{H}_{\text{SIAM}}(\tau)}. \end{aligned} \quad (20)$$

Here,  $|\psi_0^s\rangle$  is the initial (pure) state for system  $s$ , and  $\mathcal{T}$  is the (usual) time-ordering operator. Use Eq. (19) to obtain the local lattice Green function  $G_n$ .

3. Use the DMFT self-consistency condition for the Bethe lattice  $\Lambda_{n+1}(t, t') = v(t)G_n(t, t')v(t')$  to obtain the hybridization function for the next iteration.
4. Go to step 1 and iterate the steps until convergence is reached. The convergence variable can be, e.g.,  $\max |V_{0p}(t) - V_{0p,\text{prev}}(t)|$ .

From the lattice Green function we can obtain single-particle observables. In addition to the Green function, in the time-evolution we can calculate the time-dependent double occupation  $\langle d(t) \rangle = \langle \hat{n}_{1\uparrow}\hat{n}_{1\downarrow} \rangle$  which is also averaged over the systems  $\alpha$  and  $\beta$ .

### Jordan–Wigner transformation applied to the single-impurity Anderson model

The aim of the main article is to show how such DMFT steps as described above could be performed on a trapped-ion quantum computer in conjunction with a classical feedback loop. To this end, we must represent the SIAM Hamiltonian (5) with  $\mu = 0$  and  $\epsilon_{p\sigma} = 0$  in terms of spin operators that operate on the qubits. This is achieved via the Jordan–Wigner transformation, in which we map a string of  $N$  fermions onto a string of  $2N$  qubits. The relation between the fermionic creation and annihilation operators and the spin operators reads

$$\hat{a}_{p\downarrow}^\dagger = \hat{\sigma}_1^z \otimes \cdots \otimes \hat{\sigma}_{2p-2}^z \otimes \hat{\sigma}_{2p-1}^-, \quad (21)$$

$$\hat{a}_{p\uparrow}^\dagger = \hat{\sigma}_1^z \otimes \cdots \otimes \hat{\sigma}_{2p-1}^z \otimes \hat{\sigma}_{2p}^-, \quad (22)$$

$$\hat{a}_{p\sigma} = (\hat{a}_{p\sigma}^\dagger)^\dagger, \quad (23)$$

where  $\hat{\sigma}^\pm = \frac{1}{2}(\hat{\sigma}^x \pm i\hat{\sigma}^y)$ , and  $\hat{\sigma}^x$ ,  $\hat{\sigma}^y$ , and  $\hat{\sigma}^z$  are the Pauli spin operators.

We apply the transformations (21)-(23) to the SIAM Hamiltonian. The interaction term becomes

$$U(t) \left( \hat{n}_\uparrow - \frac{1}{2} \right) \left( \hat{n}_\downarrow - \frac{1}{2} \right) = \frac{1}{4} U(t) \hat{\sigma}_1^z \otimes \hat{\sigma}_2^z, \quad (24)$$

while the hybridization terms read

$$\begin{aligned}
V_{1p}^\downarrow \hat{a}_{1\downarrow}^\dagger \hat{a}_{p\downarrow} + \text{H.c.} &= \frac{1}{2} \text{Re}(V_{1p}^\downarrow) (\hat{\sigma}_1^x \otimes \hat{\sigma}_2^z \otimes \cdots \otimes \hat{\sigma}_{2p-2}^z \otimes \hat{\sigma}_{2p-1}^x + \hat{\sigma}_1^y \otimes \hat{\sigma}_2^z \otimes \cdots \otimes \hat{\sigma}_{2p-2}^z \otimes \hat{\sigma}_{2p-1}^y) \\
&+ \frac{1}{2} \text{Im}(V_{1p}^\downarrow) (\hat{\sigma}_1^y \otimes \hat{\sigma}_2^z \otimes \cdots \otimes \hat{\sigma}_{2p-2}^z \otimes \hat{\sigma}_{2p-1}^x - \hat{\sigma}_1^x \otimes \hat{\sigma}_2^z \otimes \cdots \otimes \hat{\sigma}_{2p-2}^z \otimes \hat{\sigma}_{2p-1}^y), \quad (25)
\end{aligned}$$

$$\begin{aligned}
V_{1p}^\uparrow \hat{a}_{1\uparrow}^\dagger \hat{a}_{p\uparrow} + \text{H.c.} &= \frac{1}{2} \text{Re}(V_{1p}^\uparrow) (\hat{\sigma}_2^x \otimes \hat{\sigma}_3^z \otimes \cdots \otimes \hat{\sigma}_{2p-1}^z \otimes \hat{\sigma}_{2p}^x + \hat{\sigma}_2^y \otimes \hat{\sigma}_3^z \otimes \cdots \otimes \hat{\sigma}_{2p-1}^z \otimes \hat{\sigma}_{2p}^y) \\
&+ \frac{1}{2} \text{Im}(V_{1p}^\uparrow) (\hat{\sigma}_2^y \otimes \hat{\sigma}_3^z \otimes \cdots \otimes \hat{\sigma}_{2p-1}^z \otimes \hat{\sigma}_{2p}^x - \hat{\sigma}_2^x \otimes \hat{\sigma}_3^z \otimes \cdots \otimes \hat{\sigma}_{2p-1}^z \otimes \hat{\sigma}_{2p}^y). \quad (26)
\end{aligned}$$

In order to implement the time-evolution operator in an experiment, we use the Trotter decomposition

$$e^{-i\delta t \sum_{j=1}^N \hat{h}_j} \approx \prod_{j=1}^N e^{-i\delta t \hat{h}_j}, \quad (27)$$

in which each of the terms on the right hand side can be implemented with the help of Mølmer–Sørensen gates and local and global rotations, as described in the next section.

### Implementing the SIAM Hamiltonian with Mølmer–Sørensen gates

Each exponent that consists of tensor products of  $k$  Pauli operators can be implemented (up to local rotations) with a Mølmer–Sørensen gate acting on the  $k$  qubits, one local gate acting on a single qubit, and the inverse Mølmer–Sørensen gate<sup>7,8</sup>. For example, we have the decomposition

$$\begin{aligned}
\hat{U} &= \hat{U}_{\text{MS}}^{1,k} \left( -\frac{\pi}{2}, 0 \right) \hat{U}_{1,\text{loc}}(\phi) \hat{U}_{\text{MS}}^{1,k} \left( \frac{\pi}{2}, 0 \right) \\
&= \exp(i\phi \sigma_1^z \otimes \sigma_2^x \otimes \sigma_3^x \otimes \cdots \otimes \sigma_k^x), \quad (28)
\end{aligned}$$

where the Mølmer–Sørensen gate is given by

$$\hat{U}_{\text{MS}}^{l,m}(\theta, \phi) = \exp \left[ -i \frac{\theta}{4} \left( \cos \phi \hat{S}_x + \sin \phi \hat{S}_y \right)^2 \right], \quad (29)$$

with  $\hat{S}_{x,y} = \sum_{j=l}^m \hat{\sigma}_j^{x,y}$ . The local gate in Eq. (28) reads

$$\hat{U}_{j,\text{loc}}(\phi) = \begin{cases} \exp(-i\phi \sigma_j^z) & \text{for } k = 4n - 1 \\ \exp(i\phi \sigma_j^z) & \text{for } k = 4n + 1 \\ \exp(-i\phi \sigma_j^y) & \text{for } k = 4n - 2 \\ \exp(i\phi \sigma_j^y) & \text{for } k = 4n \end{cases}, \quad n \in \mathbb{N}, \quad (30)$$

To implement a string of  $\hat{\sigma}^y$  gates instead of  $\hat{\sigma}^x$ , we use a different Mølmer–Sørensen gate, yielding the decomposition

$$\begin{aligned}
\hat{U} &= \hat{U}_{\text{MS}}^{1,k} \left( -\frac{\pi}{2}, \frac{\pi}{2} \right) \hat{U}_{1,\text{loc}}(\phi) \hat{U}_{\text{MS}}^{1,k} \left( \frac{\pi}{2}, \frac{\pi}{2} \right) \\
&= \exp(i\phi \sigma_1^z \otimes \sigma_2^y \otimes \sigma_3^y \otimes \cdots \otimes \sigma_k^y), \quad (31)
\end{aligned}$$

with the local gate

$$\hat{U}_{j,\text{loc}}(\phi) = \begin{cases} \exp(-i\phi \sigma_j^z) & \text{for } k = 4n - 1 \\ \exp(i\phi \sigma_j^z) & \text{for } k = 4n + 1 \\ \exp(i\phi \sigma_j^x) & \text{for } k = 4n - 2 \\ \exp(-i\phi \sigma_j^x) & \text{for } k = 4n \end{cases}, \quad n \in \mathbb{N}. \quad (32)$$

Any of the gates from Eqs. (25) and (26) can be obtained from Eqs. (28) and (31) by applying additional local rotations. For instance,

$$\exp(i\phi \hat{\sigma}_2^x \otimes \hat{\sigma}_3^z \otimes \cdots \otimes \hat{\sigma}_{2p-1}^z \otimes \hat{\sigma}_{2p}^x) = \exp \left( i \frac{\pi}{4} \sum_{j=4}^{2p-1} \hat{\sigma}_j^y \right) \hat{U}_{\text{MS}}^{2,2p} \left( -\frac{\pi}{2}, 0 \right) \hat{U}_{3,\text{loc}}(\phi) \hat{U}_{\text{MS}}^{2,2p} \left( \frac{\pi}{2}, 0 \right) \exp \left( -i \frac{\pi}{4} \sum_{j=4}^{2p-1} \hat{\sigma}_j^y \right), \quad (33)$$

where  $\hat{U}_{3,\text{loc}}(\phi) = \exp(-i\phi\hat{\sigma}_3^z)$  for even  $p$ , and  $\hat{U}_{3,\text{loc}}(\phi) = \exp(i\phi\hat{\sigma}_3^z)$  for odd  $p$ , with  $\phi = -\frac{1}{2}\delta t \text{Re}(V_{1p}^\dagger)$ . Similarly, e.g.,

$$\begin{aligned} & \exp(i\phi\hat{\sigma}_1^x \otimes \hat{\sigma}_2^z \otimes \cdots \otimes \hat{\sigma}_{2p-2}^z \otimes \hat{\sigma}_{2p-1}^y) \\ &= \exp\left(i\frac{\pi}{4}\hat{\sigma}_1^z\right) \exp\left(-i\frac{\pi}{4}\sum_{j=3}^{2p-2}\hat{\sigma}_j^y\right) \hat{U}_{\text{MS}}^{1,2p-1}\left(-\frac{\pi}{2}, \frac{\pi}{2}\right) \hat{U}_{2,\text{loc}}(\phi) \hat{U}_{\text{MS}}^{1,2p-1}\left(\frac{\pi}{2}, \frac{\pi}{2}\right) \exp\left(i\frac{\pi}{4}\sum_{j=3}^{2p-2}\hat{\sigma}_j^y\right) \exp\left(-i\frac{\pi}{4}\hat{\sigma}_1^z\right), \end{aligned} \quad (34)$$

where  $\hat{U}_{2,\text{loc}}(\phi) = \exp(-i\phi\hat{\sigma}_2^z)$  for even  $p$ , and  $\hat{U}_{2,\text{loc}}(\phi) = \exp(i\phi\hat{\sigma}_2^z)$  for odd  $p$ , with  $\phi = \frac{1}{2}\delta t \text{Im}(V_{1p}^\dagger)$ .

### Measuring the local Green function

An essential part of the scheme is the determination of the local non-equilibrium Green function. In this section, we propose an experimental scheme to measure it

with trapped ions. We again apply the Jordan–Wigner transformations on the  $\hat{c}$ -operators and obtain the following expressions for the different components of the Green function

$$\begin{aligned} G_{1\uparrow}^{s,>}(t,t') &= -\frac{i}{4} \left( \langle \psi_0^s | \hat{U}(0,t) (\hat{\sigma}_1^z \otimes \hat{\sigma}_2^x) \hat{U}(t,t') (\hat{\sigma}_1^z \otimes \hat{\sigma}_2^x) \hat{U}(t',0) | \psi_0^s \rangle - i \langle \psi_0^s | \hat{U}(0,t) (\hat{\sigma}_1^z \otimes \hat{\sigma}_2^z) \hat{U}(t,t') (\hat{\sigma}_1^z \otimes \hat{\sigma}_2^y) \hat{U}(t',0) | \psi_0^s \rangle \right. \\ & \quad \left. + i \langle \psi_0^s | \hat{U}(0,t) (\hat{\sigma}_1^z \otimes \hat{\sigma}_2^y) \hat{U}(t,t') (\hat{\sigma}_1^z \otimes \hat{\sigma}_2^x) \hat{U}(t',0) | \psi_0^s \rangle + \langle \psi_0^s | \hat{U}(0,t) (\hat{\sigma}_1^z \otimes \hat{\sigma}_2^y) \hat{U}(t,t') (\hat{\sigma}_1^z \otimes \hat{\sigma}_2^y) \hat{U}(t',0) | \psi_0^s \rangle \right), \end{aligned} \quad (35)$$

$$\begin{aligned} G_{1\downarrow}^{s,>}(t,t') &= -\frac{i}{4} \left( \langle \psi_0^s | \hat{U}(0,t) \hat{\sigma}_1^x \hat{U}(t,t') \hat{\sigma}_1^x \hat{U}(t',0) | \psi_0^s \rangle - i \langle \psi_0^s | \hat{U}(0,t) \hat{\sigma}_1^x \hat{U}(t,t') \hat{\sigma}_1^y \hat{U}(t',0) | \psi_0^s \rangle \right. \\ & \quad \left. + i \langle \psi_0^s | \hat{U}(0,t) \hat{\sigma}_1^y \hat{U}(t,t') \hat{\sigma}_1^x \hat{U}(t',0) | \psi_0^s \rangle + \langle \psi_0^s | \hat{U}(0,t) \hat{\sigma}_1^y \hat{U}(t,t') \hat{\sigma}_1^y \hat{U}(t',0) | \psi_0^s \rangle \right), \end{aligned} \quad (36)$$

$$\begin{aligned} G_{1\uparrow}^{s,<}(t,t') &= \frac{i}{4} \left( \langle \psi_0^s | \hat{U}(0,t') (\hat{\sigma}_1^z \otimes \hat{\sigma}_2^x) \hat{U}(t',t) (\hat{\sigma}_1^z \otimes \hat{\sigma}_2^x) \hat{U}(t,0) | \psi_0^s \rangle + i \langle \psi_0^s | \hat{U}(0,t') (\hat{\sigma}_1^z \otimes \hat{\sigma}_2^z) \hat{U}(t',t) (\hat{\sigma}_1^z \otimes \hat{\sigma}_2^y) \hat{U}(t,0) | \psi_0^s \rangle \right. \\ & \quad \left. - i \langle \psi_0^s | \hat{U}(0,t') (\hat{\sigma}_1^z \otimes \hat{\sigma}_2^y) \hat{U}(t',t) (\hat{\sigma}_1^z \otimes \hat{\sigma}_2^x) \hat{U}(t,0) | \psi_0^s \rangle + \langle \psi_0^s | \hat{U}(0,t') (\hat{\sigma}_1^z \otimes \hat{\sigma}_2^y) \hat{U}(t',t) (\hat{\sigma}_1^z \otimes \hat{\sigma}_2^y) \hat{U}(t,0) | \psi_0^s \rangle \right), \end{aligned} \quad (37)$$

$$\begin{aligned} G_{1\downarrow}^{s,<}(t,t') &= \frac{i}{4} \left( \langle \psi_0^s | \hat{U}(0,t') \hat{\sigma}_1^x \hat{U}(t',t) \hat{\sigma}_1^x \hat{U}(t,0) | \psi_0^s \rangle + i \langle \psi_0^s | \hat{U}(0,t') \hat{\sigma}_1^x \hat{U}(t',t) \hat{\sigma}_1^y \hat{U}(t,0) | \psi_0^s \rangle \right. \\ & \quad \left. - i \langle \psi_0^s | \hat{U}(0,t') \hat{\sigma}_1^y \hat{U}(t',t) \hat{\sigma}_1^x \hat{U}(t,0) | \psi_0^s \rangle + \langle \psi_0^s | \hat{U}(0,t') \hat{\sigma}_1^y \hat{U}(t',t) \hat{\sigma}_1^y \hat{U}(t,0) | \psi_0^s \rangle \right), \end{aligned} \quad (38)$$

In Eqs. (35)-(38), all time-evolution operators  $\hat{U}(t,0)$ , etc, correspond to a sequence of quantum gates obtained in the previous section.

To measure each of the summands in Eqs. (35)-(38), we introduce a probe qubit<sup>9</sup> which we couple to the system of interest. We assume that the probe qubit is prepared in the pure state  $|0\rangle$ , yielding the total density operator  $\hat{\rho}_{\text{tot}} = \hat{\rho}_{\text{sys}} \otimes |0\rangle\langle 0|$ . The combined system is then run through a Ramsey interferometer sequence described by a quantum circuit in which we first apply a Hadamard gate  $\hat{\sigma}_H$  ( $\pi/2$  pulse) on the probe qubit, followed by uni-

tary evolution of the system of interest, followed by a controlled application of Pauli gates, evolution up to the final time, another controlled application of Pauli gates, and ending with another Hadamard gate on the probe qubit (see Fig. 2 of the main text). The output state of

the qubit at the end of the Ramsey sequence is given by

$$\begin{aligned}\hat{\rho}_{\text{probe}} &= \text{Tr}_{\text{sys}} \left[ \hat{\sigma}_H \hat{T} \hat{\sigma}_H \hat{\rho}_{\text{tot}} \hat{\sigma}_H \hat{T}^\dagger \hat{\sigma}_H \right] \\ &= \frac{1 + \text{Re}[L(t, t')]}{2} |0\rangle\langle 0| - i \frac{\text{Im}[L(t, t')]}{2} |0\rangle\langle 1| \\ &\quad + i \frac{\text{Im}[L(t, t')]}{2} |1\rangle\langle 0| + \frac{1 - \text{Re}[L(t, t')]}{2} |1\rangle\langle 1|,\end{aligned}\quad (39)$$

where  $L(t, t') = \text{Tr}_{\text{sys}} \left[ \hat{T}_1^\dagger(t) \hat{T}_0(t, t') \hat{\rho}_{\text{sys}} \right]$  corresponds to one of the summands in Eqs. (35)-(38). Here, the unitary operators  $\hat{T}_0(t, t') = \langle 0 | \hat{T} | 0 \rangle = \hat{U}(t, t') \hat{\sigma} \hat{U}(t', 0)$  and  $\hat{T}_1(t) = \langle 1 | \hat{T} | 1 \rangle = \hat{\sigma}' \hat{U}(t, 0)$ , in which  $\hat{\sigma}$  and  $\hat{\sigma}'$  are Pauli operators or tensor products of Pauli operators according to Eqs. (35)-(38), act only on the system and not on the probe qubit. For example, the network in Fig. 2 of the main text corresponds to the case  $\hat{\sigma} = \hat{\sigma}_1^z \otimes \hat{\sigma}_2^x$  and  $\hat{\sigma}' = \hat{\sigma}_1^z \otimes \hat{\sigma}_2^y$ . Note that

$$\hat{\rho}_{\text{probe}} = \frac{1}{2} \left( \hat{I} + \text{Re}[L(t, t')] \hat{\sigma}_z + \text{Im}[L(t, t')] \hat{\sigma}_y \right), \quad (40)$$

where  $\hat{I}$  is the identity operator, so that we have

$$\text{Tr}_{\text{probe}} [\hat{\rho}_{\text{probe}} \hat{\sigma}_z] = \text{Re}[L(t, t')], \quad (41)$$

and

$$\text{Tr}_{\text{probe}} [\hat{\rho}_{\text{probe}} \hat{\sigma}_y] = \text{Im}[L(t, t')], \quad (42)$$

which are then experimentally measurable quantities.

In our classical simulations of the single-qubit interferometer, we try to mimic the experimental procedure, i.e., each time we compute one  $t, t'$ -point of  $L(t, t')$ , we interpret this as a measurement which collapses the state of the system. As a result, we have to start again from the origin to compute another  $t, t'$ -point. This significantly increases the effort of our classical simulations and we are able to study only small systems and relatively short time scales.

### Non-interacting system and error correction

The non-interacting impurity system comprises of SIAM Hamiltonian (5) with  $U = 0$ . We take each bath site as being independently coupled to a thermal reservoir to which it can incoherently exchange electrons with. This is described within the quantum master equation approach where the density operator  $\hat{\rho}(t)$  of the full sys-

tem obeys

$$\begin{aligned}\frac{d}{dt} \hat{\rho}(t) &= -i[\hat{H}_{\text{SIAM}}, \hat{\rho}(t)] \\ &\quad + \sum_{p>0, \sigma} \Gamma_p^- [2\hat{c}_{p\sigma} \hat{\rho}(t) \hat{c}_{p\sigma}^\dagger - \hat{\rho}(t) \hat{c}_{p\sigma}^\dagger \hat{c}_{p\sigma} - \hat{c}_{p\sigma}^\dagger \hat{c}_{p\sigma} \hat{\rho}(t)] \\ &\quad + \sum_{p>0, \sigma} \Gamma_p^+ [2\hat{c}_{p\sigma}^\dagger \hat{\rho}(t) \hat{c}_{p\sigma} - \hat{\rho}(t) \hat{c}_{p\sigma} \hat{c}_{p\sigma}^\dagger - \hat{c}_{p\sigma} \hat{c}_{p\sigma}^\dagger \hat{\rho}(t)],\end{aligned}$$

where  $\Gamma_p^\pm$  are the rates of electron ejection (-) and injection (+) to bath site  $p$ . In the case of no impurity coupling  $V_{0p}^\sigma(t) = 0$  the noise on each bath site will drive their occupancies to a steady-state value of  $n_p(\infty) = \Gamma_p^+ / (\Gamma_p^- + \Gamma_p^+)$ .

Since this model is non-interacting and has Lindblad noise terms which are linear in the electron creation and annihilation operators the master equation can be solved exactly using the so-called super-fermion formalism<sup>10</sup>. Here we use this approach to compute the impurity single-particle Green functions

$$\begin{aligned}G_\sigma^>(t, t') &= i \text{Tr}[\hat{\rho}_0 \hat{c}_{1\sigma}^\dagger(t') \hat{c}_{1\sigma}(t)], \\ G_\sigma^<(t, t') &= -i \text{Tr}[\hat{\rho}_0 \hat{c}_{1\sigma}(t) \hat{c}_{1\sigma}^\dagger(t')],\end{aligned}$$

for this system given an initial density operator  $\hat{\rho}_0$ . We focused on a quench of the Hubbard hopping parameter  $v(t)$  given by Eq. (18). The initial density operator  $\hat{\rho}_0$  was again chosen to model a  $T = 0$  half-filled paramagnetic phase<sup>4</sup>, where  $\mu = 0$ , with the impurity being in a singly occupied spin-mixed state  $\frac{1}{2}(|\uparrow\rangle\langle\uparrow| + |\downarrow\rangle\langle\downarrow|)$ , along with half the bath sites were doubly occupied  $|\uparrow\downarrow\rangle$ , and the other half empty  $|0\rangle$ . The dissipation in the bath was taken to have  $\Gamma_p^\pm = \Gamma$  so that the steady-state density of the system remains a constant unit-filling. We take the bath energies to  $\epsilon_{p\sigma}(t) = 0$  throughout.

Using the calculated  $G_\sigma^>(t, t')$  the non-equilibrium DMFT self-consistency loop was solved using (i) the standard Cholesky time-slicing proposed for a noiseless system<sup>4</sup>, explained after Eq. (17), and (ii) using a fitting procedure which attempts to correct for the effects of the bath noise. We solve numerically for the bath Green functions  $g_{p\sigma}(t, t')$  using the super-fermion approach<sup>10</sup>. To implement a noise-reduction scheme, we minimize  $\left\| \sum_p V_{0p}^\sigma(t) g_{p\sigma}(t, t') V_{0p}^\sigma(t') - \Lambda_\sigma(t, t') \right\|_F^2$  ( $\|\cdot\|_F$  is the Frobenius norm) over the  $V_{0p}^\sigma(t)$  to obtain the hybridizations corresponding to a noisy system. It is often useful to include a multiplying function of the form  $f(t, t') = \exp(-\mu|t - t'|)$  in the cost function to aid the convergence of the minimiser.

\* Electronic address: j.kreula1@physics.ox.ac.uk

<sup>1</sup> S. Wall et al., Nature Phys. **7**, 114 (2011).

<sup>2</sup> A. Georges, G. Kotliar, W. Krauth, and M. J. Rozenberg, Rev. Mod. Phys. **68**, 13 (1996).

<sup>3</sup> H. Aoki, N. Tsuji, M. Eckstein, M. Kollar, T. Oka, and P. Werner, Rev. Mod. Phys. **86**, 779 (2014).

<sup>4</sup> C. Gramsch, K. Balzer, M. Eckstein, and M. Kollar, Phys. Rev. B **88**, 235106 (2013).

- <sup>5</sup> F. A. Wolf, I. P. McCulloch, and U. Schollwöck, *Phys. Rev. B* **90**, 235131 (2014).
- <sup>6</sup> R. Blatt and C. F. Roos, *Nature Physics* **8**, 277 (2012).
- <sup>7</sup> J. Casanova, A. Mezzacapo, L. Lamata, and E. Solano, *Phys. Rev. Lett.* **108**, 190502 (2012).
- <sup>8</sup> M. Müller, K. Hammerer, Y. L. Zhou, C. F. Roos, and P. Zoller, *New Journal of Physics* **13**, 085007 (2011).
- <sup>9</sup> R. Dornier, S. R. Clark, L. Heaney, R. Fazio, J. Goold, and V. Vedral, *Phys. Rev. Lett.* **110**, 230601 (2013).
- <sup>10</sup> A. A. Dzhioev and D. S. Kosov, *J. Chem. Phys.* **134**, 044121 (2011).